IEEE Access
Multidisciplinary | Rapid Review | Open Access Journal

Received August 23, 2019, accepted September 16, 2019, date of publication September 25, 2019, date of current version October 8, 2019.

Digital Object Identifier 10.1109/ACCESS.2019.2943689

Biomechanical Evaluation of Isotropic and Shell-Core Composite Meniscal Implants for Total Meniscus Replacement: A Nonlinear Finite Element Study

DURAISAMY SHRIRAM[1], GO YAMAKO[2], ETSUO CHOSA[3], AND KARUPPPASAMY SUBBURAJ[1]

[1]Engineering Product Development (EPD) Pillar, Singapore University of Technology and Design (SUTD), Singapore 487372
[2]Department of Mechanical Design Systems, Faculty of Engineering, University of Miyazaki, Miyazaki 889-2192, Japan
[3]Department of Orthopaedic Surgery, Faculty of Medicine, University of Miyazaki, Miyazaki 889-1692, Japan

Corresponding author: Karupppasamy Subburaj (subburaj@sutd.edu.sg)

The work of D. Shriram was supported by the Singapore University of Technology and Design (SUTD) President's Doctoral Research Fellowship.

ABSTRACT Loss of meniscal function due to symptomatic meniscal tears or meniscectomy leads to biomechanical instability and articular cartilage degeneration. Synthetic meniscal implants ought to ideally restore normal joint contact mechanics and thus forfending the overlying cartilage from degeneration. The purpose of this study was to quantify the contact stresses in both tibiofemoral compartments and joint kinematics during a gait cycle after implantation of a synthetic meniscal implant. Anatomically-detailed finite element model of the knee joint was developed from magnetic resonance images of a healthy female volunteer. Gait analysis was conducted using a three-dimensional motion capture system and computed the knee joint forces and moments and quadriceps muscle forces for a complete walking cycle. The effects of a synthetic meniscal implant on joint mechanics during gait were studied by conducting finite element simulations for the following meniscus conditions: (i) intact meniscus, (ii) meniscus with complete radial posterior root tear, (iii) total meniscectomy, (iv) isotropic meniscal implant, and (v) shell-core composite meniscal implant. Posterior root tear and total meniscectomy caused substantially increased contact stresses in both tibiofemoral compartments and altered tibial kinematics. Compared to posterior root tear and total meniscectomy, the isotropic and composite meniscal implants reduced the peak contact stresses in both compartments and reduced the cartilage nodes with higher contact stresses by disseminating the load over a large surface area. The shell-core composite meniscal implant resulted in lower contact stresses in the medial compartment relative to the other meniscus conditions. This study demonstrated that posterior root tear and total meniscectomy leads to detrimental changes in joint mechanics. Superseding the injured meniscus with a synthetic meniscal implant restored the joint mechanics close to the intact meniscal state. This novel synthetic meniscal implantation approach appears to be a promising strategy for treating patients with severe meniscal injuries.

INDEX TERMS Biomechanics, finite element model, gait analysis, medical imaging, meniscal implant, musculoskeletal modeling.

I. INTRODUCTION

Meniscal injury and subsequent surgical resection of the meniscus is considered one of the risk factors for the onset of osteoarthritis (OA) [1], apparently because of changes in cartilage contact mechanics [2]. Rehabilitating or superseding the meniscus is therefore required to protect the articular cartilage from degeneration [3]. However, meniscal supersession remains a major unsolved problem in orthopaedics. While meniscal allograft transplantation

The associate editor coordinating the review of this manuscript and approving it for publication was Zhonglai Wang.

improves pain and mechanical function of the knee in patients with either partial or total meniscectomy [3], their biophysical chondroprotection of articular cartilage has not yet been demonstrated [4], [5]. The use of meniscal allograft is also constrained due to problems with the risk of developing an infection, allograft size matching and fixation, as well as allograft resorption and the likelihood of allograft rupture after transplantation [4]. Besides, the use of meniscal allograft is primarily limited to younger patients (<50 years of age) [6], while most operative treatments for treating meniscal injuries (partial or total meniscectomy) are performed in patients above the age of 45 years [7]. A synthetic meniscal implant, which overcomes the constraints of biological allografts, may be a promising alternative to allografts in treating the patients with severe meniscal injuries.

Endeavors to develop non-degradable biocompatible polymer-based meniscal implants commenced several decenniums ago, however, most of them failed to mimic the biomechanical behavior of the intact meniscus. Implantation of Dacron® and Teflon® meniscal prostheses were failed because of deposition of debris into the synovial membrane due to material wear, resulting in inflammatory synovitis [8], [9]. Implantation of polyvinyl alcohol-hydrogel (PVA-H) based meniscal implants in the sheep model resulted in a complete radial posterior root tear at the 12-month time point [10]. The challenge in the research and development of synthetic meniscal substitutes is therefore to develop a meniscal implant which mimics the biomechanical behavior of the intact meniscus, while ensuring high longevity and abrasion resistance under the influence of mechanical forces acting at the knee joint.

Polycarbonate urethane (PCU) has excellent wear properties and soft-tissue compatibility, which has been proposed as a suitable biomaterial to mimic the mechanical properties and lubrication of intact meniscus [11]–[13]. Implantation of PCU meniscal implant in sheep models showed good structural integrity and no significant changes in mechanical characteristics at the 3-months and 6-months time point [14]. Non-anatomical shaped, free-floating PCU meniscal implants were introduced for use in the human knee joint which is sutured to the native peripheral rim of the meniscus [15]. In this light, free-floating PCU meniscal implants cannot be implanted in the total medial meniscectomized patient population [16]. A computational study on PCU meniscal implant demonstrated that the contact stresses acting on the articulating surfaces and the implant displacement are sensitive to the material stiffness [17]. However, the influence of material composition on the biomechanical behavior of the meniscal implant has not been reported yet. In addition to this, no clinical or computational studies have evaluated the effect of PCU meniscal implant during the complete gait cycle or during the stance phase of gait.

The wedge-shaped geometry of the intact meniscus plays an essential role in maintaining joint congruity and mechanical stability [18]. The geometric structure of the intact meniscus has also shown to influence the mechanical stresses acting within the meniscus and the contact conditions (contact pressure and contact area) in the articulating tibial surfaces [18]–[20]. A mismatch on meniscal allograft selection of over 10% of the size of the intact meniscus will significantly influence the contact stresses in both the medial and the lateral compartments [21]. This non-physiological increase in the knee joint contact stresses is a risk factor for the onset and progression of knee OA [22]. Many commercial implants do not have horn-root attachment provision like the intact meniscus, which leads to higher meniscus extrusion and results in functional meniscectomy [15], [23]. Therefore, the shape of the meniscal implant close to the shape of the intact meniscus with intact horn-root attachment provision is necessary for the salubrious functioning of the knee joint [24], [25].

The main goal of this study was to evaluate the biomechanical changes in the knee joint for different meniscus conditions during one complete gait cycle using finite element (FE) analysis. Five difference meniscus conditions were considered for this study: (i) intact medial meniscus, (ii) medial meniscus with complete radial posterior root tear, (iii) no medial meniscus (total meniscectomy), (iv) isotropic medial meniscal implant, and (v) composite medial meniscus implant. We hypothesized that the knee joint models with isotropic and composite meniscal implants restore the normal contact mechanics in both tibiofemoral compartments and tibial kinematics. We also hypothesized that, due to material composition, the knee joint model with composite meniscal implant produces the best fit with normal contact mechanics in both compartments and joint kinematics. The current study explores the potential of FE analysis to determine whether a meniscal implant can provide chondroprotective effects on human articular cartilage when subjected to gait cycle loading and therefore prevent or delay the onset and progression of OA.

II. MATERIALS AND METHODS

The workflow of the current study is depicted in Fig. 1. A three-dimensional (3D) anatomically-detailed FE model of the knee joint was developed based on the magnetic resonance (MR) images of a skeletally mature, healthy female volunteer with no previous history of knee ailment or injury. The FE model incorporates the bone and soft tissue details of the tibiofemoral and patellofemoral components. The detailed model incorporates menisci, femoral and tibial articular cartilages, and all major ligaments and tendons. Experimentally measured tibiofemoral and patellofemoral kinematics of 23 cadaveric specimens during knee flexion [26] were used to validate the FE model. Concurrent to model development, motion analysis to determine the gait pattern of the volunteer was conducted in the gait and motion analysis laboratory. Gait cycle data, including quadriceps forces, knee forces, knee moments (valgus-varus and external-internal) and flexion-extension rotation, was used as an input in the FE model and the simulations were conducted for different meniscus conditions.

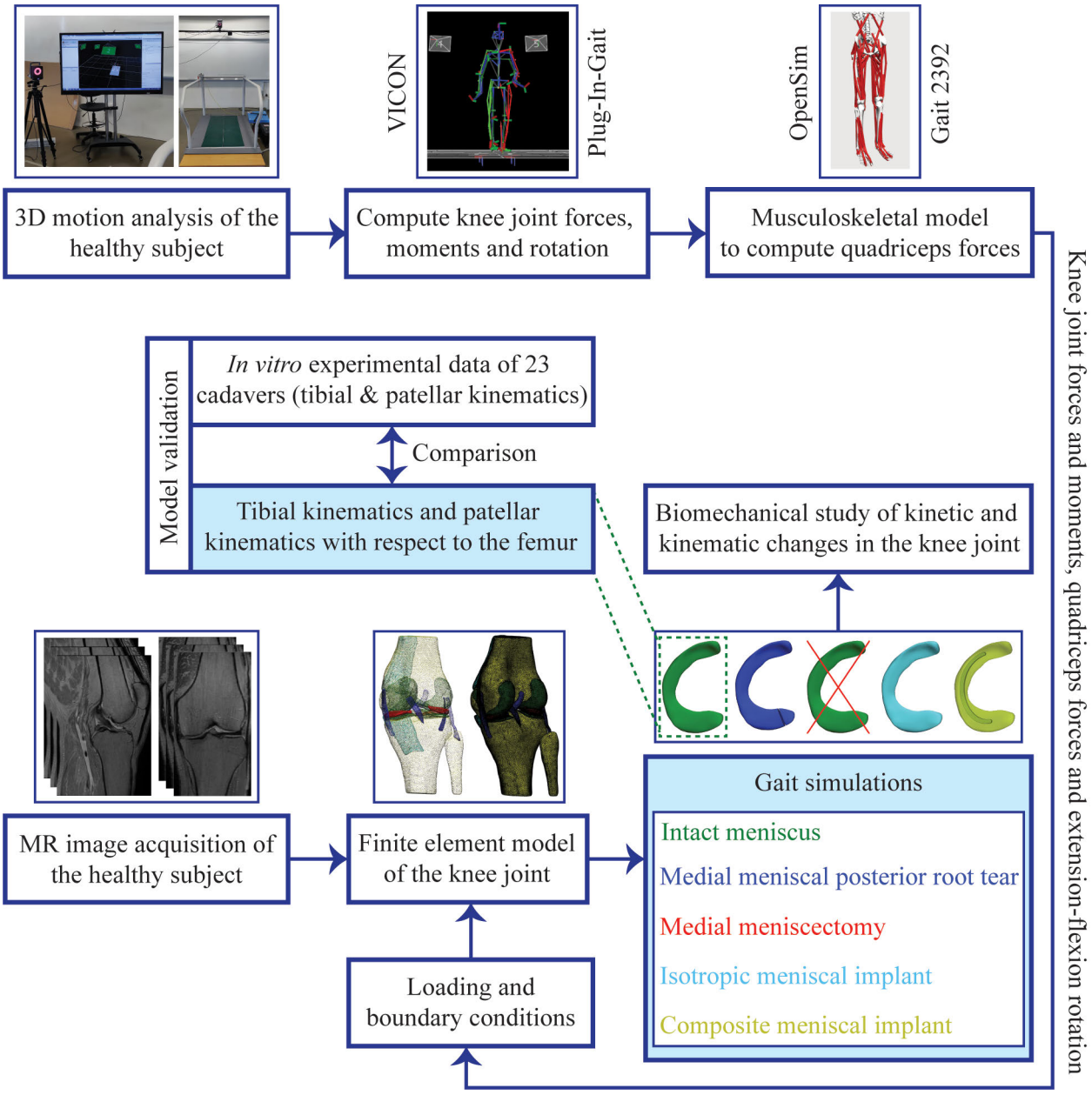

FIGURE 1. Detailed schematic describing the sequence of events undertaken in the current study.

A. KNEE JOINT GEOMETRY AND MESH GENERATION

Following approval of the institutional review board (IRB) and receiving informed consent of the subject, MR scan of the subject's right lower limb (gender: female, age: 33 years old, BMI: 21 kg/m2) was used to capture the geometry of the bones and soft tissues. Scanning was performed using a 3-T scanner (HDx, GE Healthcare, Milwaukee, WI, USA) with the subject's leg in the supine and neutral position. The protocol consisted of a fast spin-echo (FSE) sequence with the following imaging conditions: repetition time (TR) = 15 ms, echo time (TE) = 6.7 ms, flip angle = 18°, field of view (FOV) = 14 cm, matrix size = 512x512, and slice thickness = 1 mm. 3D geometry of the bones and soft tissues were reconstructed from MR images in all three anatomical reference planes (sagittal/median, coronal/frontal, transverse/axial) using Mimics (Materialise NV, Leuven, Belgium). The final solid model of the knee joint (Fig. 2A) consisted of femur, tibia, fibula, patella, menisci (medial and lateral), articular cartilages (femoral, tibial and patellar), cruciate ligaments (anterior and posterior), collateral ligaments (medial and lateral), anterolateral ligament, and tendons (quadriceps and patellar).

These geometries were imported to ABAQUS (Dassault Systèmes Simulia Corp., Providence, RI, USA) to develop

TABLE 1. Mesh and element characteristics of each knee joint substructure in the final mesh model used for the analysis.

Knee substructure		Mesh characteristics		
		Element type	Element size (mm)	Total number of elements
Femur bone		Rigid, 3-node, triangular facet (all bony structures)	2	174265
Tibia bone			2	112826
Patella bone			2	43189
Fibula bone			2	31411
Articular cartilage	Femoral	Deformable, 10-node, tetrahedral (all soft tissues and implants)	1	171612
	Tibial		1	79610
	Patellar		1	58372
Meniscus	Medial		1	65270
	Lateral		1	89627
Medial meniscal implant	Isotropic		1	65270
	Composite shell		1	49725
	Composite core		1	14745
Cruciate ligament	Anterior		0.5	120533
	Posterior		0.5	130519
Collateral ligament	Medial		0.5	77918
	Lateral		0.5	104664
Anterolateral ligament			0.5	47283
Tendon	Patellar		1	103495
	Quadriceps		1	132457

the FE model of the knee joint (Fig. 2A). The bony structures were meshed using 3D rigid 3-noded triangular elements (R3D3 from ABAQUS mesh library) and all the soft tissues and the meniscal implants were meshed using 10-noded second-order quadratic tetrahedral elements (C3D10 from ABAQUS mesh library). A mesh convergence study was carried out to optimize mesh density. To verify the convergence of the FE mesh model and to ensure the mesh density does not influence the model estimations, all the soft tissues were meshed in different element sizes to develop multiple mesh models ranging from coarse to refined. The model's estimation of peak contact pressure induced in the medial compartment under the application of an axial compressive load of 1000 N was analyzed. The element sizes of the knee joint soft tissues were considered optimized when the model's estimation resulted <5% difference when compared to that of the model with very refined mesh. Donahue *et al.* utilized a kindred methodology to determine the mesh density for the knee joint soft tissues [27]. The element details of each joint substructure in the final FE model are tabulated in Table I. Other simulated substructures in the final mesh model, including meniscal horn attachments, meniscofemoral ligaments, transverse meniscomeniscal ligaments, patellofemoral ligaments, and capsular ligaments were modeled as two-noded one-dimensional (1D) spring elements.

B. GAIT AND MOTION ANALYSIS

The gait pattern of the subject was analyzed in the gait and motion analysis laboratory at the Singapore University of Technology and Design, Singapore. The subject completed five standard gait trials walking at a self-selected speed of approximately 1.5 m/s along the treadmill walkway. 3D kinematic data of 49 markers collected using a 12-camera VICON MX motion capture system (Oxford Metrics Ltd., Oxford, UK) was synchronized with kinetic data collected using two AMTI treadmill force platforms (AMTI, Newton, MA, USA). Kinematic and kinetic data were collected at 120 Hz and 1080 Hz, respectively. The kinetic data from the treadmill force platforms were low pass filtered at 15 Hz cut off frequency (3rd order, zero-lag Butterworth) to reduce the effect of mechanical noise [28]. VICON Nexus Plug-In-Gait module (version 2.9, Oxford Metrics Ltd., Oxford, UK) was used to compute and output the kinetic and kinematic data including joint rotations (using inverse kinematics approach) and joint forces and moments (using inverse dynamics approach). Quadriceps muscle force, estimated using OpenSim (version 4, SimTK, Stanford, CA, USA), was required to model the patellofemoral articulation. The generic OpenSim Gait 2392 musculoskeletal model [29] was used to compute the individual muscle forces. Inverse kinematics data computed using VICON Nexus were the primary inputs for the musculoskeletal model. Muscle forces of vastus lateralis, vastus medialis, rectus femoris, and vastus intermedius were computed by using the static optimization [30] tool in OpenSim, and the algebraic sum of these forces gives the quadriceps muscle forces [31]. The final gait data input for the FE knee joint model included knee translational forces (Fig. 2B), knee moments (Fib. 2C) and quadriceps muscle forces (Fig. 2D). The contributing effects of other muscles and connective tissues were considered in the knee joint FE model by applying only 50% of the estimated valgus-varus and external-internal moments acting at the knee [32].

C. CONSTRAINTS AND LOADING AND BOUNDARY CONDITIONS

The bony structures, including the femur, tibia, patella, and fibula were modeled as rigid bodies to optimize computational cost without compromising model validity, while

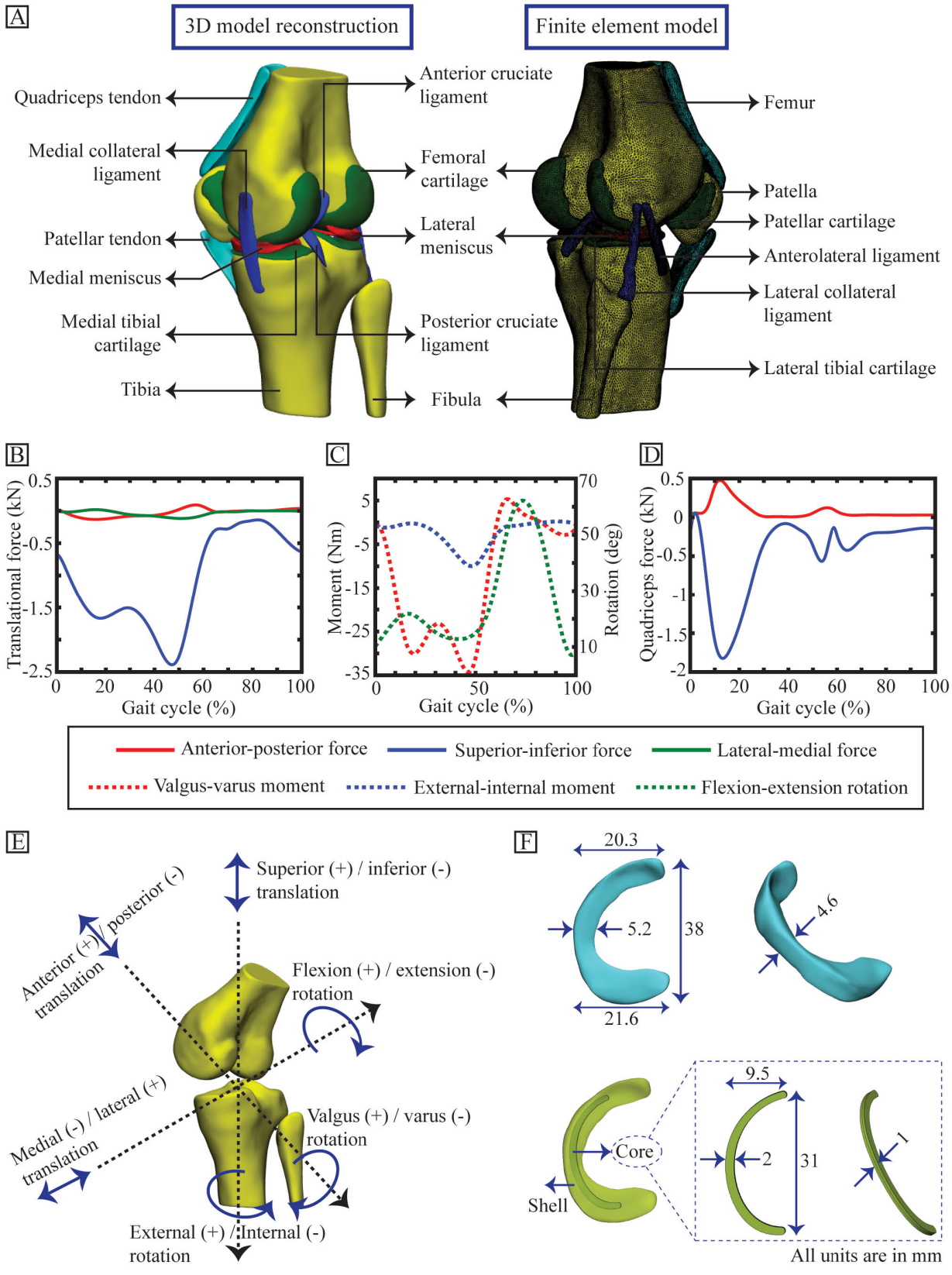

FIGURE 2. (A) 3D MRI reconstructed model and finite element mesh model of the knee joint. (B) Applied knee joint forces (anterior-posterior, superior-inferior, and lateral-medial components). (C) Applied knee joint moments (valgus-varus and external-internal components) and flexion-extension rotations. (D) Applied quadriceps muscle forces (anterior-posterior and superior-inferior components). (E) Representation of six degrees of freedom kinematics of the knee joint. (F) The geometry of isotropic meniscal implant (top) and composite meniscal implant (bottom).

the other knee substructures were modeled as deformable bodies [17], [33]. A 3D tangential (frictionless sliding) surface-to-surface contact pattern was defined between all articulating surfaces of the knee joint FE model [27], [33], [34]. The master-slave general contact assignment in ABAQUS was defined for 18 contact pairs in the FE model: collateral ligaments-proximal femur, collateral ligaments-distal tibia, anterolateral ligament-proximal femur, anterolateral ligament-distal tibia, cruciate ligaments-proximal femur, cruciate ligaments-distal tibia, anterior cruciate ligament-posterior cruciate ligament, femoral articular cartilage-menisci, menisci-tibial articular cartilage, femoral articular cartilage-tibial articular cartilage, and femoral articular cartilage-patellar articular cartilage [27], [33], [34]. The insertion points of the ligaments and tendons identified from the MR images were used for simulating the ligament-bone and tendon-bone attachments. All degrees of freedom of the tibial bottom nodes were fixed during analysis, while the proximal femur was only constrained in flexion. The patella was free to displace and rotate in all degrees of freedom. The six degrees of freedom kinematics of the knee joint (Fig. 2E) were expressed using non-orthogonal joint coordinate system [35]. The influence of the tension in the ligaments and tendons at rest was considered in the FE knee model before the implementation of gait cycle loading by applying a pre-strain. The cruciate ligaments (anterior and posterior) were pre-strained at 5%, while the collateral ligaments (medial and lateral), anterolateral ligament and tendons (quadriceps and patellar) were pre-strained at 4% [36]. The subject-specific gait cycle data input (Fig. 2B-2D) was implemented into the FE model through the gait point, located in between the medial and lateral epicondyles of the femur [17], [37]. The dynamic effects of the FE mesh are sensitive to the loading frequency. For the loading frequency (~0.5 Hz) that was applied in the current study, dynamic effects of the FE mesh remained nugatory in all the simulation steps.

D. MENISCUS CONDITIONS AND IMPLANT GEOMETRY

Five knee models with various medial meniscus conditions were created in the current study (Fig. 1).

1) Knee model with the native intact meniscus, where the geometry was reconstructed from the acquired MR images as discussed afore.
2) Knee model with complete radial posterior root tear in the medial meniscus, where the type 2 root tear [38] was numerically simulated within 9 mm of the root attachment.
3) Medial meniscectomized knee model, where the complete medial meniscus was excluded from the simulation.
4) Knee model with an isotropic meniscal implant, where the geometry was adopted from the intact meniscus (Fig. 2F) to simulate the effects of the subject-specific anatomical shaped isotropic meniscal implant.
5) Knee model with a composite meniscal implant, where the shell geometry was adopted from the intact meniscus and the core geometry was scaled and resized based on the shell (Fig. 2F). The composite meniscal implant shell was modelled with a thickness of 1.5 mm. The composite meniscal implant shell and composite meniscal implant core were constrained using the ''TIE'' constraint in ABAQUS, which constrains the relative motion between the two structures.

E. MATERIAL PROPERTIES

Articular cartilages were modeled as neo-Hookean hyperelastic isotropic material (nonlinear) with the strain energy density as a function of elastic volume strain (J_{el}) and first strain invariant ($\bar{I}_1$):

$$U = C_{10}(\bar{I}_1 - 3) + \frac{1}{D_1}(J_{el} - 1)^2 \tag{1}$$

In equation (1), C_{10} and D_1 are neo-Hookean material constants, and the values of these constants ($C_{10} = 0.86$ MPa and $D_1 = 0.048$ MPa^{-1})

were calculated using ABAQUS by fitting the hyperelastic constants to experimental data [39].

The native meniscus (medial and lateral) was modeled as transversely isotropic hyperelastic material by incorporating the Holzapfel-Gasser-Ogden (HGO) material model [40], [41] with the strain energy density function:

$$U = C_{10}(\bar{I}_1 - 3) + \frac{1}{D_1}\left(\frac{(J_{el})^2 - 1}{2} - \ln J_{el}\right) + \frac{k_1}{2k_2}\left(\exp\left[k_2\left\langle\bar{E}_\alpha\right\rangle^2\right] - 1\right) \tag{2}$$

with

$$\bar{E}_\alpha = \kappa(\bar{I}_1 - 3) + (1 - 3\kappa)(\bar{I}_{4(\alpha\alpha)} - 1) \tag{3}$$

In equation (2), $\bar{I}_{4(\alpha\alpha)}$ are the pseudo-invariants of the symmetric modified Cauchy-Green strain tensor, which is required to model the effects of relatively stiff collagen fibers. The terms C_{10}, D_1 , k_1 , k_2 and κ denote material parameters and the values of these parameters (Table II) were calculated by fitting the hyperelastic parameters to the experimentally measured biomechanical properties [42], [43] using ABAQUS. The parameter κ describes the fiber orientation and dispersion and the value of this parameter ranges from 0 (perfect fiber alignment and no dispersion) to 1/3 (fibers are randomly dispersed). In this study, the meniscal fibers were aligned circumferentially ($\kappa = 0$) to resist circumferential stresses during gait cycle loading [44].

The constitutive model and failure criteria of transversely isotropic hyperelastic neo-Hookean material [45], to model the ligaments and tendons, were implemented in ABAQUS/Explicit solver through a user-defined VUMAT subroutine (Fig. 3). The strain energy density function, shown in equation (4), is a function of non-collagenous matrix material (neo-Hookean parameters) and reinforcement material (fiber family parameter ($R(\lambda)$)).

$$U = C_{10}(\bar{I}_1 - 3) + \frac{1}{D_1}(J_{el} - 1)^2 + R(\lambda) \tag{4}$$

TABLE 2. Material parameters used for modeling the medial and lateral meniscus [42], [43]. Parameters C_{10} and D_1: neo-Hookean constants, k_1 and k_2: HGO coefficients, and κ: Fiber dispersion and orientation level.

Knee substructure	C_{10} (MPa)	D_1 (MPa^{-1})	k_1	k_2	κ
Medial meniscus	1	5e-3	5.0	0.9	0
Lateral meniscus	1	5e-3	8.5	1.6	0

TABLE 3. Material parameters used for modeling the cruciate and collateral ligaments, anterolateral ligament and tendons [33], [46], [47]. Parameters C_{10} and D_1: neo-Hookean constants, C_3 : Exponential stress factor, C_4 : Collagen fiber un-crimping rate, C_5 : Elastic modulus of straightened fibers, and $\bar{\lambda}$: Maximum value of fiber stretch beyond which the fibers straighten.

Knee substructure		C_{10} (MPa)	D_1 (MPa^{-1})	C_3 (MPa)	C_4 (-)	C_5 (MPa)	$\bar{\lambda}$ (-)
Cruciate ligament	Anterior	1.95	0.007	0.014	116.22	535.1	1.046
	Posterior	3.25	0.004	0.120	87.18	431.1	1.035
Collateral ligament	Medial	1.44	0.001	0.57	48.0	467.1	1.063
	Lateral	1.44	0.001	0.57	48.0	467.1	1.063
Anterolateral ligament		1.44	0.001	0.57	48.0	467.1	1.063
Tendon	Patellar	2.75	0.005	0.065	115.89	777.56	1.042
	Quadriceps	2.75	0.005	0.065	115.89	777.56	1.042

The fiber family function $R(\lambda)$ denotes the collagen fiber stiffness and fulfills the following conditions:

$$\lambda \frac{dR(\lambda)}{d\lambda} = \begin{cases} 0, & \lambda \leq 1 \\ C_3(\exp(C_4(\lambda - 1)) - 1), & 1 < \lambda < \bar{\lambda} \\ C_5\lambda + C_6, & \lambda \geq \bar{\lambda} \end{cases} \quad (5)$$

where λ denotes the local fiber stretch. The collagen fibers resist compression due to close packing in crystals and would buckle when subjected to compressive load ($\lambda \leq 1$). When the collagen fibers were stretched to some value less than $\bar{\lambda}$ ($1 < \lambda < \bar{\lambda}$), the fiber stiffness increases exponentially with increasing stretch. When the collagen fibers were stretched beyond $\bar{\lambda}$ ($\lambda \geq \bar{\lambda}$), the fibers straighten out and the fiber stiffness increases linearly. The material coefficients C_3, C_4, C_5 and C_6 denote the scale parameter that scales the exponential stress, collagen fiber un-crimping rate, Young's modulus of straightened fibers and the factor which ensures stress continuation at $\bar{\lambda}$. In ligaments and tendons, the collagen fibers were oriented parallel to the principal geometrical axis to transmit tensile forces. The collagen fibers did not damage in all the simulation steps because the fiber strain was always less than the threshold value. The material coefficients for modeling the ligaments and tendons (Table III) were calculated by fitting the material constants to experimental data [33], [46], [47].

The meniscal horn attachments were modeled using nonlinear incompressible spring elements with a combined spring stiffness of $k = 350$ N/mm for each horn [48]. The meniscofemoral (anterior and posterior) and meniscomeniscal (transverse) ligaments were modelled using incompressible nonlinear spring elements with spring stiffness of $k = 49$ N/mm and $k = 400$ N/mm , respectively [49]–[51]. The patellofemoral ligaments (medial and lateral) were modelled using nonlinear spring elements with total spring stiffness of $k = 49$ N/mm for each ligament [52], [53]. The capsular ligaments including medial capsular, lateral capsular, oblique popliteal and arcuate popliteal were modelled using incompressible nonlinear spring elements with spring stiffness of $k = 15$ N/mm, $k = 14$ N/mm, $k = 28$ N/mm, and $k = 34$ N/mm, respectively [54]–[57]. The material for isotropic meniscal implant (type 80A, E=11 MPa, Bionate® grade II polycarbonate urethane (PCU), DSM Biomedical Inc., Berkeley, CA, USA), composite meniscal implant shell (Bionate® grade II PCU type 80A, E=11 MPa) and composite meniscal implant core (Bionate® grade II PCU type 55D, E=17 MPa) were modelled as isotropic hyperelastic neo-Hookean material ($C_{10} = 1.84$ MPa and $D_1 = 0.011$ MPa^{-1} for isotropic meniscal implant and composite meniscal implant shell; $C_{10} = 2.85$ MPa and $D_1 = 0.007$ MPa^{-1} for composite meniscal implant core) with a Poisson coefficient of $\nu = 0.49$. The density of all the soft tissues and implants was assumed to be 1×10^{-9} ton/mm^3.

III. RESULTS

The peak compression forces occurred at 25% (referred hereafter as 1st peak) and 80% (referred hereafter as 2nd peak) of the stance phase of gait (Fig. 2B).

A. MEDIAL COMPARTMENT CONTACT MECHANICS

Posterior root tear and total medial meniscectomy increased the peak contact pressure on the medial tibial plateau by 15%/18% (1st peak/2nd peak) and 12%/18% (1st peak/2nd peak), respectively, when compared with the intact meniscus condition (Figs. 4A). The same increasing trend was observed in peak compressive stress and peak shear stress (Figs. 4C, 4E). Intact meniscus distributed the contact stresses over a large surface area, however, posterior root tear and total medial meniscectomy reduced the contact surface area and increased the number of nodes in the anterior-tibial region of the medial tibial plateau with higher contact stresses (Figs. 4B, 4D, 4F). Relative to the intact meniscus condition, posterior root tear and total medial meniscectomy decreased

FIGURE 3. Flowchart describing the implementation of user-defined VUMAT material subroutine in ABAQUS/Explicit finite element solver.

the contact area on the medial tibial plateau by 61%/42% (1st peak/2nd peak) and 63%/61% (1st peak/2nd peak), respectively (Fig. 4G).

Isotropic meniscal implant and composite meniscal implant restored the medial compartment contact mechanics to that in the knee joint with intact meniscus (Figs. 4A-G). The isotropic and composite meniscal implants reduced the peak contact pressure by 10%/21% (1st peak/2nd peak) and 18%/30% (1st peak/2nd peak), respectively, when compared with total medial meniscectomy (Fig. 4A). The same behavior was observed in peak compressive stress and peak shear stress (Figs. 4C, 4E). Relative to total medial meniscectomy, both isotropic and composite meniscal implants redistributed the contact stresses over a large surface area and reduced the number of nodes on the medial tibial plateau with higher contact stresses (Figs. 4B, 4D, 4F). The isotropic and composite meniscal implants increased the contact area on the medial tibial plateau by 40%/33% (1st peak/2nd peak) and 42%/38% (1st peak/2nd peak), respectively, when compared with total medial meniscectomy (Fig. 4G).

B. LATERAL COMPARTMENT CONTACT MECHANICS

Posterior root tear and total medial meniscectomy led to increase in the peak contact pressure on the lateral tibial plateau by 35%/42% (1st peak/2nd peak) and 43%/53% (1st peak/2nd peak), respectively, when compared with the intact meniscus (Fig. 5A). The same behavior was observed in peak compressive stress and peak shear stress (Fig. 5C, 5E). Relative to the intact meniscus, posterior root tear and total medial meniscectomy decreased the contact area on the lateral tibial plateau by 20%/43% (1st peak/2nd peak) and 24%/56% (1st peak/2nd peak), respectively, and increased the cartilage nodes with higher contact stresses (Fig. 5B, 5D, 5F, 5G).

Implantation of isotropic and composite medial meniscal implants significantly improved the contact mechanics of the lateral tibial plateau. The isotropic and composite meniscal implants reduced the peak contact pressure on the lateral tibial plateau by 42%/26% (1st peak/2nd peak) and 31%/13% (1st peak/2nd peak), respectively, when compared with total medial meniscectomy (Fig. 5A). The same reducing trend was observed in peak compressive stress and peak shear stress (Fig. 5C, 5E). Compared with total medial meniscectomy, the isotropic and composite meniscal implants increased the contact area on the lateral tibial plateau by 22%/94% (1st peak/2nd peak) and 16%/83% (1st peak/2nd peak), respectively, and reduced the cartilage nodes with higher contact stresses (Fig. 5B, 5D, 5F, 5G).

C. TIBIAL KINEMATICS RELATIVE TO THE FEMUR

Anterior-posterior translation of the tibia, increased in association with the posterior root tear and total medial meniscectomy conditions, was restored by implanting isotropic and composite meniscal implants (Fig. 6A). Posterior root tear and total medial meniscectomy resulted in a maximum increase in anterior-posterior translation of up to 2.8 mm and 8.1 mm, respectively, when compared with the intact meniscus. The change was conspicuous during the loading response phase, mid-stance phase and terminal swing phase of the gait cycle. Inferior-superior translation of the tibia relative to the femur was almost similar for all meniscus conditions during the stance phase of gait (Fig. 6B). A maximum increase in lateral-medial tibial translation of up to 8 mm and 8.6 mm was observed in the knee joint models with posterior root tear and total medial meniscectomy, respectively, when compared with the knee joint model with intact meniscus (Fig. 6C). The change was conspicuous throughout all phases of the gait cycle. The isotropic and composite meniscal implants restored the lateral-medial tibial translation to that observed in the intact meniscus condition. Relative to the intact meniscus, the tibial translations observed in the isotropic and composite meniscal implants were close in range, and the best fit in tibial translations was observed in the isotropic meniscal implant condition (Figs. 6A-C).

Posterior root tear and total medial meniscectomy resulted in a maximum increase in the valgus-varus tibial rotation of up to 3.5 degrees and 3.9 degrees, respectively, when compared with the intact meniscus (Fig. 6D). The change was prominent during the terminal stance phase and swing phase of the gait cycle. Isotropic and composite meniscal implants restored the valgus-varus rotation of the tibia to that observed in the knee joint model with the intact meniscus. Relative to the intact meniscus, posterior root tear and total medial meniscectomy resulted in a maximum increase in the external-internal rotation of the tibia of up to 12 degrees and 17 degrees, respectively (Fig. 6E). The change was prominent during the stance phase and terminal swing phase of the gait cycle. The increasing trend in the external-internal rotation of the tibia pronounced in the knee joint models with posterior root tear and total medial meniscectomy was restored by the knee joint models implanted with isotropic and composite meniscal implants. The flexion-extension rotation of the tibia relative to the femur was similar for all meniscus conditions because this rotation was implemented in the FE model as a boundary condition (Fig. 6F). The best fit in tibial rotations was observed in the composite meniscal implant when compared with the intact meniscus condition (Figs. 6D, 6E).

IV. DISCUSSION

The current study evaluated the biomechanical performance of synthetic, anatomical shaped, isotropic and composite medial meniscal implants, in comparison with that of the intact meniscus. For the first time, subject-specific FE model of the knee joint with the physiological loading conditions was used to evaluate the functional performance of the meniscal implant during a complete gait. Compared to total medial meniscectomy, the isotropic and composite meniscal implants reduced the peak contact stresses in both tibiofemoral compartments and the number of cartilage nodes with higher contact stresses by distributing the load over a large surface area. Some of the significant observations from the current study were that (1) the isotropic and composite

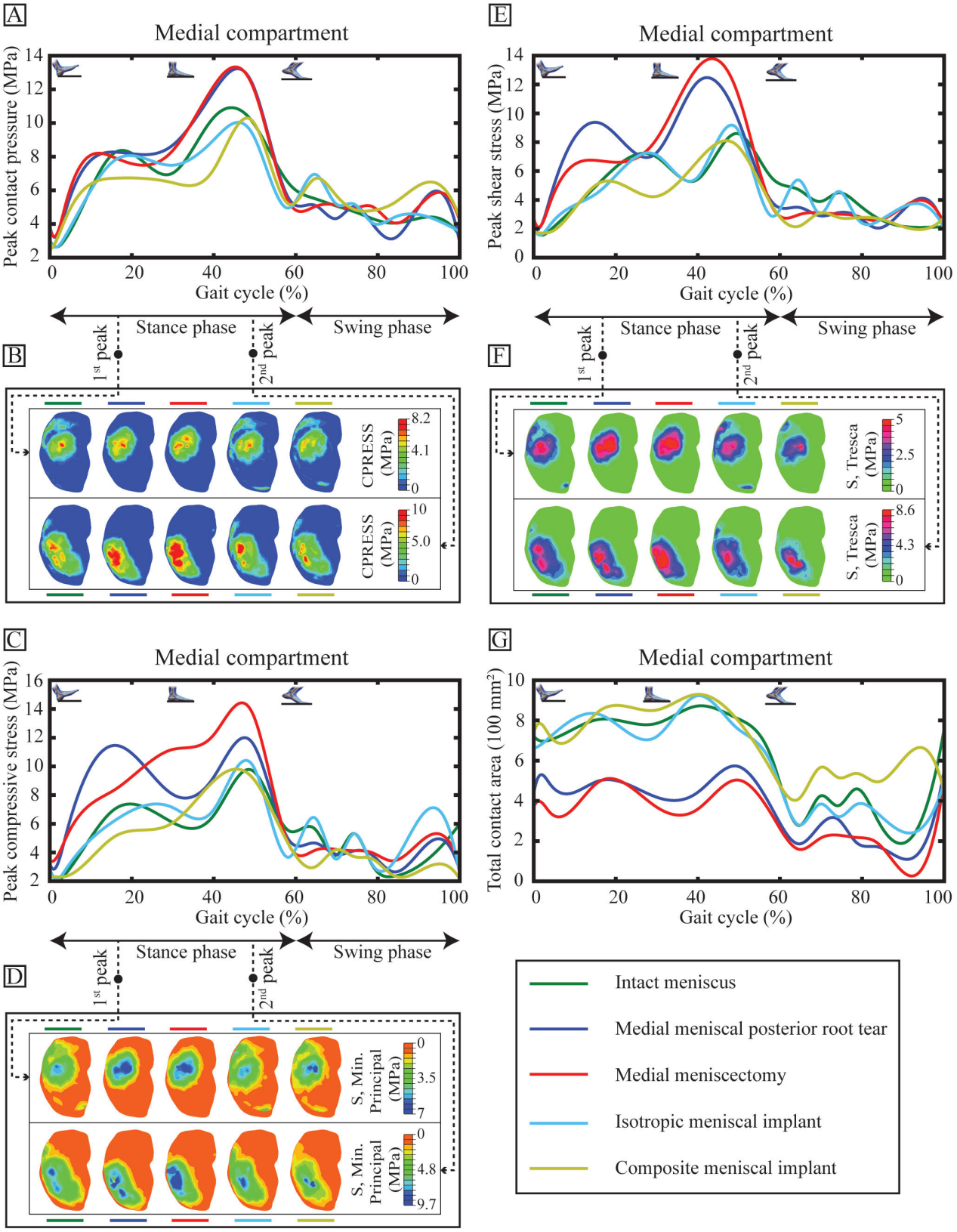

FIGURE 4. **Comparison of medial compartment biomechanics between knee joint finite element models with different meniscus conditions: (A) peak contact pressure during one complete gait, (B) distribution of contact pressures on the medial tibial cartilage at 25% and 80% of the stance phase of gait, (C) peak compressive stress during one complete gait, (D) distribution of minimum principal (compressive) stresses on the medial tibial cartilage surface at 25% and 80% of the stance phase of gait, (E) peak shear stress during one complete gait, (F) distribution of shear stresses on the medial tibial cartilage surface at 25% and 80% of the stance phase of gait, and (G) total contact area during one complete gait.**

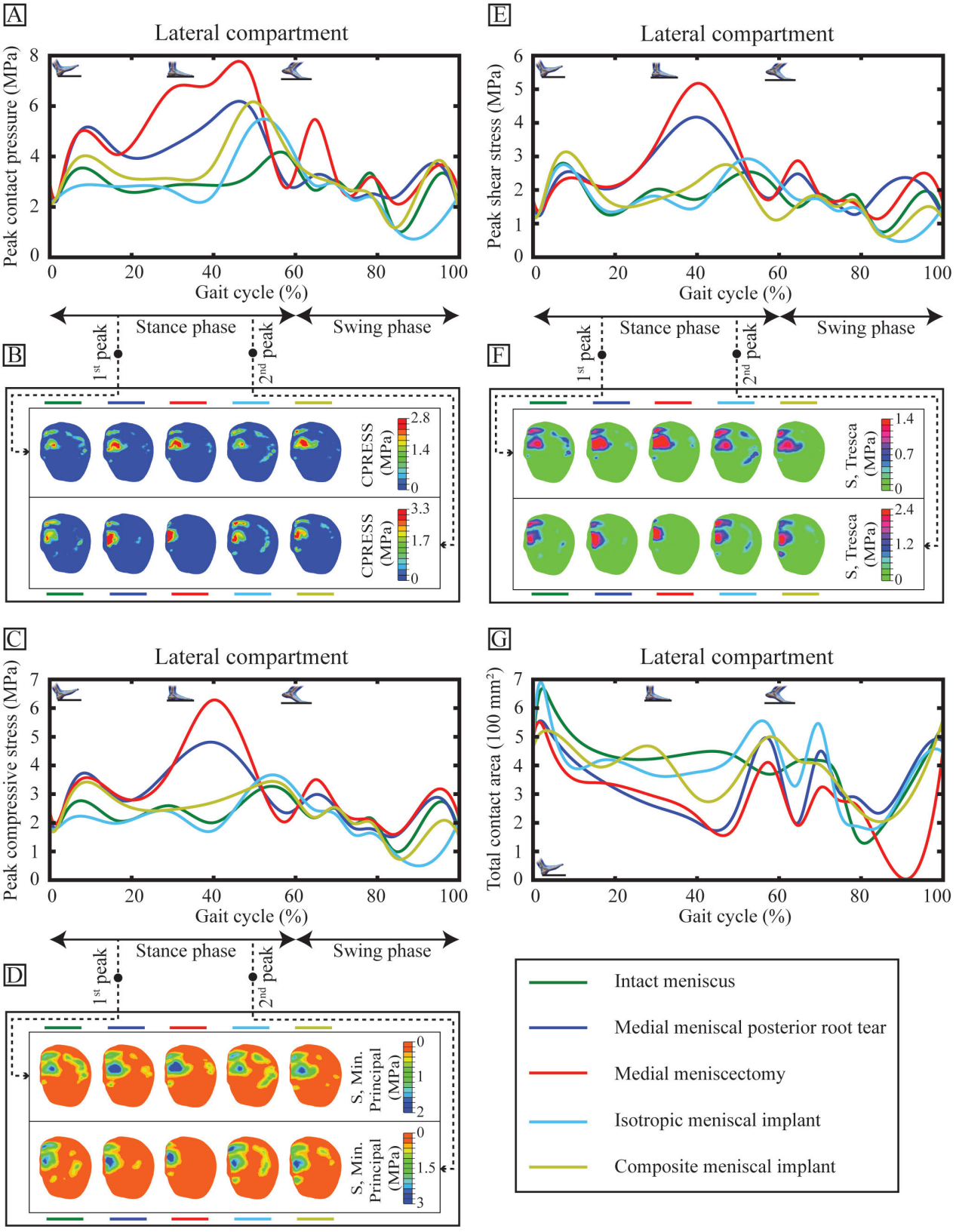

FIGURE 5. Comparison of lateral compartment biomechanics between knee joint finite element models with different meniscus conditions: (A) peak contact pressure during one complete gait, (B) distribution of contact pressures on the lateral tibial cartilage at 25% and 80% of the stance phase of gait, (C) peak compressive stress during one complete gait, (D) distribution of minimum principal (compressive) stresses on the lateral tibial cartilage surface at 25% and 80% of the stance phase of gait, (E) peak shear stress during one complete gait, (F) distribution of shear stresses on the lateral tibial cartilage surface at 25% and 80% of the stance phase of gait, and (G) total contact area during one complete gait.

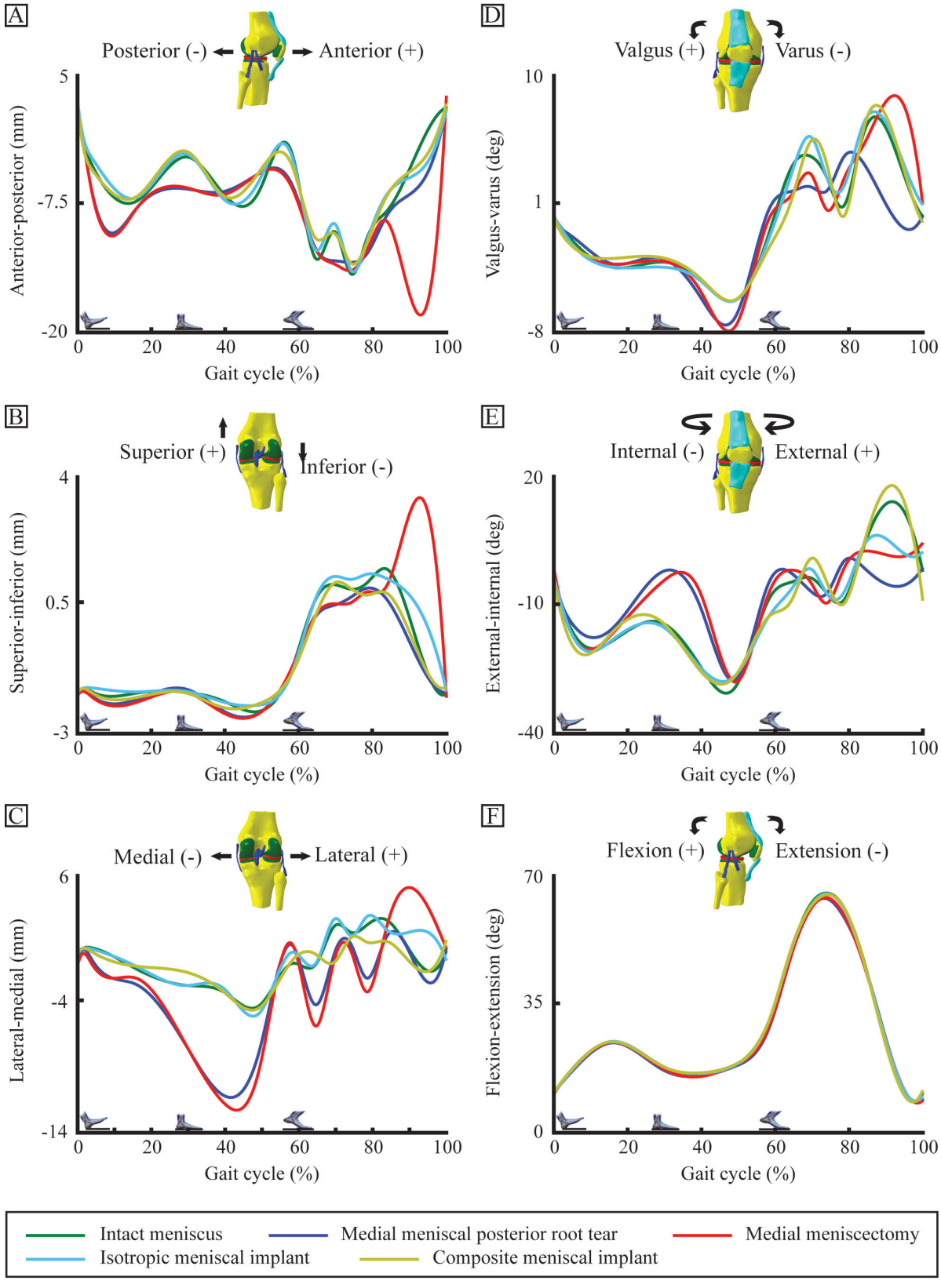

FIGURE 6. **Tibial kinematics with respect to the femur during one complete gait cycle for different meniscus conditions: (A) anterior-posterior translation, (B) superior-inferior translation, (C) lateral-medial translation, (D) valgus-varus rotation, (E) external-internal rotation, and (F) flexion-extension rotation. Flexion-extension rotations for all meniscus conditions remain the same because they were applied as a boundary condition to the finite element model.**

meniscal implants restored the normal joint kinematics and contact conditions in both tibiofemoral compartments, (2) the knee joint model with isotropic meniscal implant resulted in a maximum reduction of contact stresses in the lateral compartment and produced the best fit with the normal tibial translational kinematics, and (3) the knee joint model with composite meniscal implant resulted in a maximum reduction of contact stresses in the medial compartment and produced the best fit with the normal tibial rotational kinematics.

The intrinsic difficulties in cadaveric experiments to study the contact stresses and joint kinematics have made FE analysis a reliable numerical tool to study the biomechanical changes of the knee joint. Accurate representation of substructure geometry, appropriate material model, physiological constraints and loading conditions, and proper validation against controlled experimental data are the key elements in constructing a valid and reliable FE model to study the stresses and strains in the complex anatomical structures. The tibial kinematics and patellar kinematics relative to the femur, computed using the FE model, were compared with the *in vitro* experimental data (experiments conducted on 23 lower extremities of fresh-frozen cadavers) [26] to validate the FE model. The tibial translations and rotations observed in the knee joint FE model with intact meniscus were within the range of that measured in the cadaveric experiments (Figs. 7A-F). The FE model predicted an external-internal rotation of up to -14 degrees at 70 degrees flexion, which is in the range of that measured in the cadaveric experiments (-12.75 $\pm$ 5.55 degrees at 70 degrees flexion) (Fig. 7E). The patellofemoral kinematics computed using the FE model was also within the measured physiological range of the patellar translations and rotations (Figs. 7G-L).

The peak contact pressure and the total contact area estimated in this study also falls within the range of values reported in the literature. The knee joint model with the intact meniscus estimated a peak contact pressure of 7 MPa/11 MPa (1^{st} peak/2^{nd} peak) and 2.8 MPa/4 MPa (1^{st} peak/2^{nd} peak) on the medial and lateral tibial plateau, respectively. These values are in line with the cadaveric experimental studies that reported a peak contact pressure of 6-11 MPa/5-10.5 MPa (medial/lateral compartment) and 11-17 MPa/4-6 MPa (medial/lateral compartment) during single-limb stance (axial load of 1150 N) [58] and loading response phase (axial load of 2.25 times the bodyweight) [59], respectively. Thambyah *et al*. reported that the peak contact pressure measured in the medial compartment in all cadaveric specimens was over two times higher than that in the lateral compartment during the heel strike event of the stance phase of gait [59]. This finding is consistent with the results estimated by our FE model. In our numerical study, the contact area on the medial tibial plateau was always higher than that on the lateral tibial plateau during all events of gait, which is in line with the findings reported by Gilbert *et al*. [60]. The knee joint model with the intact meniscus estimated a total contact area of 800 mm^2/820 mm^2 (1^{st} peak/2^{nd} peak) and 446 mm^2/430 mm^2 (1^{st} peak/2^{nd} peak) on the medial and lateral tibial plateau, respectively. These values are in line with a cadaveric experimental study that reported a total contact area of 650$\pm$190 mm^2 and 500$\pm$90 mm^2 in the medial and lateral compartments, respectively, under an axial load of 1000 N [61]. Furthermore, the total contact area reported by FE-based studies [62], [63] was similar to that estimated in our study.

The current study demonstrated that the knee joint models with posterior root tear and total medial meniscectomy resulted in increased contact stresses in both the medial and lateral compartments and altered tibial kinematics. Numerous experimental and computational studies have also shown that the total medial meniscectomy causes a significant increase in the peak contact pressure and a decrease in the total contact area of the medial tibial plateau [2], [17], [25], [64]–[68]. In our study, the total medial meniscectomy decreased the contact area on the medial tibial plateau by 63%/61% (1^{st} peak/2^{nd} peak) relative to the intact meniscus, and this change is consistent with the values reported by Chen *et al*. ($\sim$60%) [25] and Paletta *et al*. ($\sim$55-65%) [68]. Medial meniscal extrusion of over 3 mm was observed in patients with a complete radial posterior root tear of the medial meniscus and found an association with articular cartilage degeneration, synovial inflammation, and osteophyte formation [69]. A cadaveric study has demonstrated, based on the biomechanical changes in contact conditions and tibial kinematics, that a complete radial posterior root tear of the medial meniscus resulted in functional meniscectomy [64]. These findings, in addition to the availability and compatibility constraints of the biological allografts [4], [5], led us to focus on design and evaluation of synthetic meniscal alternatives for restoring the normal joint biomechanics.

The shell-core polymer composite structure consists of a soft shell and stiff core, in which the soft shell is responsible for loading distribution, and the stiff core is required to maintain the stability of the structure [70]. Based on this theory, we hypothesized that the knee joint model with a shell-core composite meniscal implant would best mimic the biomechanical performance of the intact meniscus. In our study, we observed both the isotropic and composite meniscal implants restore the normal functionality of the knee joint. Implantation of composite meniscal implant resulted in lower contact stresses in the medial compartment and better mimic the normal tibial rotational kinematics. On the other hand, implantation of isotropic meniscal implant resulted in lower contact stresses in the lateral compartment and produced the best fit with the normal tibial translational kinematics. The superior performance of the isotropic meniscal implant in the lateral compartment contact mechanics and tibial translational kinematics may be attributed to the increased proportion of low-stiffness material when compared to the composite meniscal implant. This observation seems partially against our hypothesis since we expected the composite meniscal implant to produce the best fit with normal contact mechanics in both the compartments and tibial kinematics. However, the differences in contact stresses in the lateral

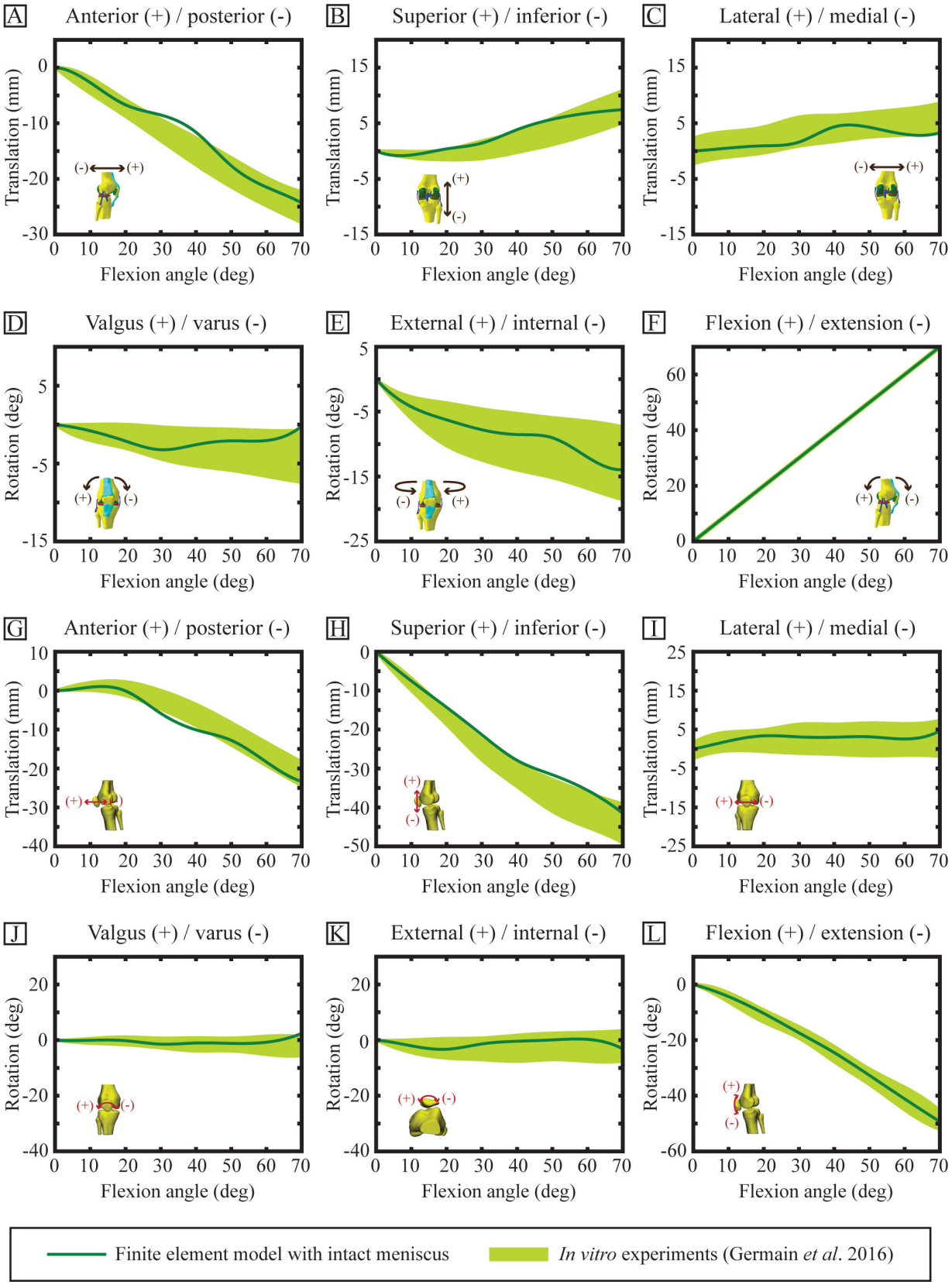

FIGURE 7. **Comparison of numerically simulated and experimentally measured tibiofemoral and patellofemoral kinematics relative to the femur during the range of motion.**

compartment and tibial translational kinematics between the isotropic meniscal implant and composite meniscal implant were observed to be minimal.

The implant design with the provision for horn attachment will provide structural integrity and stability and restore the normal functioning of the knee joint [24], [25]. Transplantation of meniscal allograft without fixation of meniscal horn attachments resulted in functional meniscectomy [25], [68]. The geometry of NUsurface® meniscal implant (ACTIVE IMPLANTS LLC, TN, USA) designed for animal study in sheep model was anatomically shaped [14], while a free-floating disc-shaped meniscal implant geometry was designed for use in human subjects [15]. NUsurface® meniscal implant designed for human subjects do not necessitate fixation to bone or adjacent cartilage, which may lead to loosening and dislocation of the implant [71]. Given the demand for the synthetic meniscal implant for use in the growing number of clinical applications [71], immediate care must be given to improve the geometry of the meniscal implants. This study evaluated two design configurations of the meniscal implant and both designs address the complications of non-anatomic design features by incorporating the anatomical shaped geometry with provision for anterior and posterior horn attachments. The design configurations of meniscal implant proposed in this study may be more suitable for patients with severe meniscal deficiency. A detailed comparative biomechanical FE study is therefore required to evidently prove that the anatomical shaped isotropic and shell-core composite meniscal implants offer superior biomechanical characteristics when compared to the NUsurface® free-floating meniscal implant.

This study has a few limitations that need to be considered while interpreting the findings. All our results and conclusions were based on the FE analysis of one subject's data. However, we would relish to accentuate that this is a methodological research study showing that it is possible to use the validated FE model to evaluate the biomechanical effects of meniscal substitutes for total meniscus replacement. This methodology can further be applied for clinical investigations involving more number of subjects. The intersubject variability may affect the absolute values of contact stresses and tibial kinematics, however, the main conclusions derived in this study will not change [72], [73]. The depth-dependent mechanical and biochemical properties of the articular cartilage were not considered in this study, which may affect the behavior of contact stresses on the articular cartilage [74], [75]. However, for the loading frequency (∼0.5 Hz) that was applied in the current study, the cartilage tissue will not have sufficient time to discharge the interstitial fluid and therefore exhibits the same behavior as the elastic material 76]. The location of the meniscal implant insertion site was determined using MR images and confirmed by two orthopaedic consultants, without a chance for experimentally verifying the anatomical landmark of the insertion site. The variation in implant positioning may lead to altered joint biomechanics and the effects have not yet been studied in detail [4]. It has been clinically shown that one-third of patients with total medial meniscectomy experience decreased range of motion [77]. Since the gait characteristics of the healthy subject were measured in this study, the knee models with different meniscus conditions were simulated using the same loading and boundary conditions. Despite these limitations, the comparison between the knee joint models with different meniscus conditions provided a relative estimate of the differences in contact stresses and tibial kinematics that would be expected *in vivo* due to total meniscus replacement with a synthetic meniscal implant.

V. CONCLUSION

In summary, we have developed a subject-specific finite element model of the knee joint to estimate the contact mechanics and joint kinematics of a synthetic meniscal implant under physiological loading conditions. This study could help explain the development of knee OA due to increased contact stresses and altered joint kinematics caused by the loss of meniscal tissue. Implantation of isotropic and shell-core composite meniscal implants restored the contact mechanics and joint kinematics close to the intact meniscal state. The shell-core composite meniscal implant resulted in maximum reduction of contact stresses in the medial compartment relative to the other meniscus conditions and produces the best fit with the normal tibial rotational kinematics. As a clinical consequence, this novel synthetic meniscal implantation approach appears to be a promising strategy for treating patients with severe meniscal injuries. The model developed in this study shed light on the knowledge of joint mechanics after injury or repair, and therefore can also assist in the clinical evaluation of other alternative repair techniques.

ETHICS DECLARATIONS

This study was approved by the Institutional Review Board of the Singapore University of Technology and Design (SUTD) and the subject gave written informed consent.

REFERENCES

[1] S. N. Edd, N. J. Giori, and T. P. Andriacchi, "The role of inflammation in the initiation of osteoarthritis after meniscal damage," *J. Biomech.*, vol. 48, no. 8, pp. 1420–1426, 2015.
[2] S. J. Lee, K. J. Aadalen, P. Malaviya, E. P. Lorenz, J. K. Hayden, J. Farr, R. W. Kang, and B. J. Cole, "Tibiofemoral contact mechanics after serial medial meniscectomies in the human cadaveric knee," *Amer. J. Sports Med.*, vol. 34, no. 8, pp. 1334–1344, 2006.
[3] R. Lawton, P. Thompson, and T. Spalding, "Meniscal repair and replacement," *Orthopaedics Trauma*, vol. 33, no. 2, pp. 109–118, Apr. 2019.
[4] B. J. Cole, T. R. Carter, and S. A. Rodeo, "Allograft meniscal transplantation: Background, techniques, and results," *J. Bone Joint Surg.*, vol. 84, no. 7, pp. 1236–1250, 2002.
[5] N. A. Smith, B. Parkinson, C. E. Hutchinson, M. L. Costa, and T. Spalding, "Is meniscal allograft transplantation chondroprotective? A systematic review of radiological outcomes," *Knee Surg., Sports Traumatol., Arthroscopy*, vol. 24, no. 9, pp. 2923–2935, Sep. 2016.
[6] M. De Bruycker, P. C. M. Verdonk, and R. C. Verdonk, "Meniscal allograft transplantation: A meta-analysis," *SICOT-J.*, vol. 3, p. 33, Apr. 2017.
[7] G. D. Abrams, R. M. Frank, A. K. Gupta, J. D. Harris, F. M. McCormick, and B. J. Cole, "Trends in Meniscus Repair and Meniscectomy in the United States, 2005–2011," *Amer. J. Sports Med.*, vol. 41, no. 10, pp. 2333–2339, Jul. 2013.

[8] K. Messner, L. S. Lohmander, and J. Gillquist, "Cartilage mechanics and morphology, synovitis and proteoglycan fragments in rabbit joint fluid after prosthetic meniscal substitution," *Biomaterials*, vol. 14, no. 3, pp. 163–168, 1993.

[9] K. Messner, "Meniscal substitution with a teflon-periosteal composite graft: A rabbit experiment," *Biomaterials*, vol. 15, no. 3, pp. 223–230, 1994.

[10] B. T. Kelly, W. Robertson, H. G. Potter, X.-H. Deng, A. S. Turner, S. Lyman, R. F. Warren, and S. A. Rodeo, "Hydrogel meniscal replacement in the sheep knee: Preliminary evaluation of chondroprotective effects," *Amer. J. Sports Med.*, vol. 35, no. 1, pp. 43–52, Jan. 2007.

[11] I. Khan, N. Smith, E. Jones, D. S. Finch, and R. E. Cameron, "Analysis and evaluation of a biomedical polycarbonate urethane tested in an *in vitro* study and an ovine arthroplasty model. Part I: Materials selection and evaluation," *Biomaterials*, vol. 26, no. 6, pp. 621–631, 2005.

[12] I. Khan, N. Smith, E. Jones, D. S. Finch, and R. E. Cameron, "Analysis and evaluation of a biomedical polycarbonate urethane tested in an in vitro study and an ovine arthroplasty model. Part II: *In vivo* investigation," *Biomaterials*, vol. 26, no. 6, pp. 633–643, 2005.

[13] S. C. Scholes, A. Unsworth, and E. Jones, "Polyurethane unicondylar knee prostheses: Simulator wear tests and lubrication studies," *Phys. Med. Biol.*, vol. 52, no. 1, pp. 197–212, Dec. 2006.

[14] G. Zur, E. Linder-Ganz, J. J. Elsner, J. Shani, O. Brenner, G. Agar, E. B. Hershman, S. P. Arnoczky, F. Guilak, and A. Shterling, "Chondroprotective effects of a polycarbonate-urethane meniscal implant: Histopathological results in a sheep model," *Knee Surg., Sports Traumatol. Arthroscopy*, vol. 19, no. 2, pp. 255–263, Feb. 2011.

[15] J. J. Elsner, S. Portnoy, G. Zur, F. Guilak, A. Shterling, and E. Linder-Ganz, "Design of a free-floating polycarbonate-urethane meniscal implant using finite element modeling and experimental validation," *J. Biomech. Eng.*, vol. 132, no. 9, 2010, Art. no. 095001.

[16] T. De Coninck, J. J. Elsner, E. Linder-Ganz, M. Cromheecke, M. Shemesh, W. Huysse, R. Verdonk, K. Verstraete, and P. Verdonk, "*In-vivo* evaluation of the kinematic behavior of an artificial medial meniscus implant: A pilot study using open-MRI," *Clin. Biomech.*, vol. 29, no. 8, pp. 898–905, 2014.

[17] D. Shriram, G. P. Kumar, F. Cui, Y. H. D. Lee, and K. Subburaj, "Evaluating the effects of material properties of artificial meniscal implant in the human knee joint using finite element analysis," *Sci. Rep.*, vol. 7, no. 1, 2017, Art. no. 6011.

[18] A. J. S. Fox, A. Bedi, and S. A. Rodeo, "The basic science of human knee menisci: Structure, composition, and function," *Sports Health, Multidisciplinary Approach*, vol. 4, no. 4, pp. 340–351, Jul. 2012.

[19] T. L. H. Donahue, M. L. Hull, M. M. Rashid, and C. R. Jacobs, "The sensitivity of tibiofemoral contact pressure to the size and shape of the lateral and medial menisci," *J. Orthopaedic Res.*, vol. 22, no. 4, pp. 807–814, 2004.

[20] J. R. Meakin, N. G. Shrive, C. B. Frank, and D. A. Hart, "Finite element analysis of the meniscus: The influence of geometry and material properties on its behaviour," *Knee*, vol. 10, no. 1, pp. 33–41, 2003.

[21] M. Dienst, P. E. Greis, B. J. Ellis, K. N. Bachus, and R. T. Burks, "Effect of lateral meniscal allograft sizing on contact mechanics of the lateral tibial plateau: An experimental study in human cadaveric knee joints," *Amer. J. Sports Med.*, vol. 35, no. 1, pp. 34–42, Jan. 2007.

[22] I. D. McDermott and A. A. Amis, "The consequences of meniscectomy," *J. Bone Joint Surg. Brit. Volume*, vol. 88-B, no. 12, pp. 1549–1556, 2006.

[23] E. Linder-Ganz, J. J. Elsner, A. Danino, F. Guilak, and A. Shterling, "A novel quantitative approach for evaluating contact mechanics of meniscal replacements," *J. Biomech. Eng.*, vol. 132, no. 2, 2010, Art. no. 024501.

[24] M. M. Alhalki, S. M. Howell, and M. L. Hull, "How three methods for fixing a medial meniscal autograft affect tibial contact mechanics," *Amer. J. Sports Med.*, vol. 27, no. 3, pp. 320–328, 1999.

[25] M. I. Chen, T. P. Branch, W. C. Hutton, and D. Sc, "Is it important to secure the horns during lateral meniscal transplantation? A cadaveric study," *Arthroscopy, J. Arthroscopic Rel. Surg.*, vol. 12, no. 2, pp. 174–181, 1996.

[26] F. Germain, P. Y. Rohan, G. Rochcongar, P. Rouch, P. Thoreux, H. Pillet, and W. Skalli, "Role of ligaments in the knee joint kinematic behavior: Development and validation of a finite element model," in *Computational Biomechanics for Medicine*, G. Joldes, B. Doyle, A. Wittek, P. Nielsen, and K. Miller, Eds. Cham, Switzerland: Springer, 2016, pp. 15–26. [Online]. Available: https://link.springer.com/chapter/10.1007/978-3-319-28329-6_2

[27] T. L. H. Donahue, M. L. Hull, M. M. Rashid, and C. R. Jacobs, "A finite element model of the human knee joint for the study of tibio-femoral contact," *J. Biomech. Eng.*, vol. 124, no. 3, pp. 273–280, 2002.

[28] E. S. Matijevich, L. M. Branscombe, L. R. Scott, and K. E. Zelik, "Ground reaction force metrics are not strongly correlated with tibial bone load when running across speeds and slopes: Implications for science, sport and wearable tech," *PLoS ONE*, vol. 14, no. 1, 2019, Art. no. e0210000.

[29] S. L. Delp, F. C. Anderson, A. S. Arnold, P. Loan, A. Habib, C. T. John, E. Guendelman, and D. G. Thelen, "OpenSim: Open-source software to create and analyze dynamic simulations of movement," *IEEE Trans. Biomed. Eng.*, vol. 54, no. 11, pp. 1940–1950, Nov. 2007.

[30] S. Heintz and E. M. Gutierrez-Farewik, "Static optimization of muscle forces during gait in comparison to EMG-to-force processing approach," *Gait Posture*, vol. 26, no. 2, pp. 279–288, 2007.

[31] A. A. Ali, E. M. Mannen, P. J. Rullkoetter, and K. B. Shelburne, "*In vivo* comparison of medialized dome and anatomic patellofemoral geometries using subject-specific computational modeling," *J. Orthopaedic Res.*, vol. 36, no. 7, pp. 1910–1918, Jul. 2018.

[32] K. S. Halonen, M. E. Mononen, J. S. Jurvelin, J. Töyräs, A. Klodowski, J.-P. Kulmala, and R. K. Korhonen, "Importance of patella, quadriceps forces, and depthwise cartilage structure on knee joint motion and cartilage response during gait," *J. Biomech. Eng.*, vol. 138, no. 7, 2016, Art. no. 071002.

[33] E. Peña, B. Calvo, M. A. Martínez, and M. Doblaré, "A three-dimensional finite element analysis of the combined behavior of ligaments and menisci in the healthy human knee joint," *J. Biomech.*, vol. 39, no. 9, pp. 1686–1701, 2006.

[34] M. Z. Bendjaballah, A. Shirazi-Adl, and D. J. Zukor, "Finite element analysis of human knee joint in varus-valgus," *Clin. Biomech.*, vol. 12, no. 3, pp. 139–148, 1997.

[35] S. Grood and W. Suntay, "A joint coordinate system for the clinical description of three-dimensional motions: Application to the knee," *J. Biomech. Eng.*, vol. 105, no. 2, pp. 136–144, 1983.

[36] F. M. Gantoi, M. A. Brown, and A. A. Shabana, "Finite element modeling of the contact geometry and deformation in biomechanics applications," *J. Comput. Nonlinear Dyn.*, vol. 8, no. 4, 2013, Art. no. 041013.

[37] A. Cappozzo, F. Catani, U. D. Croce, and A. Leardini, "Position and orientation in space of bones during movement: Anatomical frame definition and determination," *Clin. Biomech.*, vol. 10, no. 4, pp. 171–178, 1995.

[38] C. M. LaPrade, E. W. James, T. R. Cram, J. A. Feagin, L. Engebretsen, and R. F. LaPrade, "Meniscal root tears: A classification system based on tear morphology," *Amer. J. Sports Med.*, vol. 43, no. 2, pp. 363–369, Dec. 2014.

[39] D. E. Shepherd and B. B. Seedhom, "The 'instantaneous' compressive modulus of human articular cartilage in joints of the lower limb," *Rheumatology*, vol. 38, no. 2, pp. 124–132, 1999.

[40] G. A. Holzapfel, T. C. Gasser, and R. W. Ogden, "A new constitutive framework for arterial wall mechanics and a comparative study of material models," *J. Elasticity Phys. Sci. Solids*, vol. 61, nos. 1–3, pp. 1–48, Jul. 2000.

[41] T. C. Gasser, R. W. Ogden, and G. A. Holzapfel, "Hyperelastic modelling of arterial layers with distributed collagen fibre orientations," *J. R. Soc. Interface*, vol. 3, no. 6, pp. 15–35, 2006.

[42] M. Tissakht and A. M. Ahmed, "Tensile stress-strain characteristics of the human meniscal material," *J. Biomech.*, vol. 28, no. 4, pp. 411–422, 1995.

[43] E. K. Danso, J. T. A. Mäkelä, P. Tanska, M. E. Mononen, J. T. J. Honkanen, J. S. Jurvelin, J. Töyräs, P. Julkunen, and R. K. Korhonen, "Characterization of site-specific biomechanical properties of human meniscus—Importance of collagen and fluid on mechanical nonlinearities," *J. Biomech.*, vol. 48, no. 8, pp. 1499–1507, 2015.

[44] M. Freutel, F. Galbusera, A. Ignatius, and L. Dürselen, "Material properties of individual menisci and their attachments obtained through inverse FE-analysis," *J. Biomech.*, vol. 48, no. 8, pp. 1343–1349, 2015.

[45] J. A. Weiss, B. N. Maker, and S. Govindjee, "Finite element implementation of incompressible, transversely isotropic hyperelasticity," *Comput. Methods Appl. Mech. Eng.*, vol. 135, no. 1, pp. 107–128, 1996.

[46] D. L. Butler, M. Y. Sheh, D. C. Stouffer, V. A. Samaranayake, and M. S. Levy, "Surface strain variation in human patellar tendon and knee cruciate ligaments," *J. Biomech. Eng.*, vol. 112, no. 1, pp. 38–45, 1990.

[47] J. C. Gardiner and J. A. Weiss, "Subject-specific finite element analysis of the human medial collateral ligament during valgus knee loading," *J. Orthopaedic Res.*, vol. 21, no. 6, pp. 1098–1106, 2003.

[48] D. F. Villegas, J. A. Maes, S. D. Magee, and T. L. H. Donahue, "Failure properties and strain distribution analysis of meniscal attachments," *J. Biomech.*, vol. 40, no. 12, pp. 2655–2662, 2007.

[49] T. Kusayama, C. D. Harner, G. J. Carlin, J. W. Xerogeanes, and B. A. Smith, "Anatomical and biomechanical characteristics of human meniscofemoral ligaments," *Knee Surg., Sports Traumatol., Arthroscopy*, vol. 2, no. 4, pp. 234–237, Dec. 1994.
[50] A. C. Abraham, J. T. Moyer, D. F. Villegas, G. M. Odegard, and T. L. H. Donahue, "Hyperelastic properties of human meniscal attachments," *J. Biomech.*, vol. 44, no. 3, pp. 413–418, Feb. 2011.
[51] T. L. H. Donahue, M. L. Hull, M. M. Rashid, and C. R. Jacobs, "How the stiffness of meniscal attachments and meniscal material properties affect tibio-femoral contact pressure computed using a validated finite element model of the human knee joint," *J. Biomech.*, vol. 36, no. 1, pp. 19–34, 2003.
[52] K. E. Kim, S.-L. Hsu, and S. L.-Y. Woo, "Tensile properties of the medial patellofemoral ligament: The effect of specimen orientation," *J. Biomech.*, vol. 47, no. 2, pp. 592–595, Jan. 2014.
[53] A. M. Merican, S. Sanghavi, F. Iranpour, and A. A. Amis, "The structural properties of the lateral retinaculum and capsular complex of the knee," *J. Biomech.*, vol. 42, no. 14, pp. 2323–2329, Oct. 2009.
[54] H. Ishigooka, T. Sugihara, K. Shimizu, H. Aoki, and K. Hirata, "Anatomical study of the popliteofibular ligament and surrounding structures," *J. Orthopaedic Sci.*, vol. 9, no. 1, pp. 51–58, 2004.
[55] T. Sugita and A. A. Amis, "Anatomic and biomechanical study of the lateral collateral and popliteofibular ligaments," *Amer. J. Sports Med.*, vol. 29, no. 4, pp. 466–472, Jul. 2001.
[56] R. F. LaPrade, A. Tso, and F. A. Wentorf, "Force measurements on the fibular collateral ligament, popliteofibular ligament, and popliteus tendon to applied loads," *Amer. J. Sports Med.*, vol. 32, no. 7, pp. 1695–1701, Oct. 2004.
[57] R. F. LaPrade, P. M. Morgan, F. A. Wentorf, S. Johansen, and L. Engebretsen, "The anatomy of the posterior aspect of the knee: An anatomic study," *J. Bone Joint Surg.*, vol. 89, no. 4, pp. 758–764, 2007.
[58] A. Thambyah, "Contact stresses in both compartments of the tibiofemoral joint are similar even when larger forces are applied to the medial compartment," *Knee*, vol. 14, no. 4, pp. 336–338, 2007.
[59] A. Thambyah, J. C. H. Goh, and S. D. De, "Contact stresses in the knee joint in deep flexion," *Med. Eng. Phys.*, vol. 27, no. 4, pp. 329–335, 2005.
[60] S. Gilbert, T. Chen, I. D. Hutchinson, D. Choi, C. Voigt, R. F. Warren, and S. A. Maher, "Dynamic contact mechanics on the tibial plateau of the human knee during activities of daily living," *J. Biomech.*, vol. 47, no. 9, pp. 2006–2012, 2014.
[61] T. Fukubayashi and H. Kurosawa, "The contact area and pressure distribution pattern of the knee: A study of normal and osteoarthrotic knee joints," *Acta Orthopaedica Scandinavica*, vol. 51, nos. 1–6, pp. 871–879, 1980.
[62] B. Zielinska and T. L. H. Donahue, "3D finite element model of meniscectomy: Changes in joint contact behavior," *J. Biomech. Eng.*, vol. 128, no. 1, pp. 115–123, Sep. 2005.
[63] Y. Dong, G. Hu, Y. Dong, Y. Hu, and Q. Xu, "The effect of meniscal tears and resultant partial meniscectomies on the knee contact stresses: A finite element analysis," *Comput. Methods Biomech. Biomed. Eng.*, vol. 17, no. 13, pp. 1452–1463, Oct. 2014.
[64] R. Allaire, M. Muriuki, L. Gilbertson, and C. D. Harner, "Biomechanical consequences of a tear of the posterior root of the medial meniscus: Similar to total meniscectomy," *J. Bone Joint Surg. Amer.*, vol. 90, no. 9, pp. 1922–1931, 2008.
[65] M. E. Baratz, F. H. Fu, and R. Mengato, "Meniscal tears: The effect of meniscectomy and of repair on intraarticular contact areas and stress in the human knee: A preliminary report," *Amer. J. Sports Med.*, vol. 14, no. 4, pp. 270–275, Jul. 1986.
[66] P. S. Walker and M. J. Erkiuan, "The role of the menisci in force transmission across the knee," *Clin. Orthopaedics Rel. Res.*, vol. 109, pp. 184–192, Jun. 1975.
[67] D. Shriram, G. Yamako, E. Chosa, Y. H. D. Lee, and K. Subburaj, "Effects of a valgus unloader brace in the medial meniscectomized knee joint: A biomechanical study," *J. Orthopaedic Surg. Res.*, vol. 14, no. 1, 2019, Art. no. 44.
[68] G. A. Paletta, T. Manning, E. Snell, R. Parker, and J. Bergfeld, "The effect of allograft meniscal replacement on intraarticular contact area and pressures in the human knee: A biomechanical study," *Amer. J. Sports Med.*, vol. 25, no. 5, pp. 692–698, Sep. 1997.
[69] D. B. Lerer, H. R. Umans, M. X. Hu, and M. H. Jones, "The role of meniscal root pathology and radial meniscal tear in medial meniscal extrusion," *Skeletal Radiol.*, vol. 33, no. 10, pp. 569–574, Oct. 2004.
[70] H. Wang, L. Yang, and G. L. Rempel, "Preparation of poly(methyl methacrylate)/polystyrene/poly(acrylonitrile-co-butadiene) tri-layer core–shell nanoparticles and their postpolymerization modification via catalytic latex hydrogenation," *RSC Adv.*, vol. 5, no. 55, pp. 44483–44491, 2015.
[71] L. Verhaeghe and K. Boeren, "A rare complication after synthetic meniscus replacement," *J. Belg. Soc. Radiol.*, vol. 102, no. 1, p. 63, Oct. 2018.
[72] L. P. Räsänen, M. E. Mononen, M. T. Nieminen, E. Lammentausta, J. S. Jurvelin, and R. K. Korhonen, "Implementation of subject-specific collagen architecture of cartilage into a 2D computational model of a knee joint—Data from the osteoarthritis initiative (OAI)," *J. Orthopaedic Res.*, vol. 31, no. 1, pp. 10–22, 2013.
[73] R. Parween, D. Shriram, R. E. Mohan, Y. H. D. Lee, and K. Subburaj, "Methods for evaluating effects of unloader knee braces on joint health: A review," *Biomed. Eng. Lett.*, vol. 9, no. 2, pp. 153–168, 2019.
[74] R. Shirazi, A. Shirazi-Adl, and M. Hurtig, "Role of cartilage collagen fibrils networks in knee joint biomechanics under compression," *J. Biomech.*, vol. 41, no. 16, pp. 3340–3348, 2008.
[75] M. E. Mononen, M. T. Mikkola, P. Julkunen, R. Ojala, M. T. Nieminen, J. S. Jurvelin, and R. K. Korhonen, "Effect of superficial collagen patterns and fibrillation of femoral articular cartilage on knee joint mechanics—A 3D finite element analysis," *J. Biomech.*, vol. 45, no. 3, pp. 579–587, 2012.
[76] G. A. Ateshian, B. J. Ellis, and J. A. Weiss, "Equivalence between short-time biphasic and incompressible elastic material responses," *J. Biomech. Eng.*, vol. 129, no. 3, pp. 405–412, Jun. 2007.
[77] P. Abdon, M. S. Turner, H. Pettersson, A. Lindstrand, A. Stenstroêm, and A. J. G. Swanson, "A long-term follow-up study of total meniscectomy in children," *Clin. Orthopaedics Rel. Res.*, vol. 257, pp. 166–170, Aug. 1990.

DURAISAMY SHRIRAM received the bachelor's degree in mechanical engineering from Anna University, India, in 2011, the master's degree in mechanical engineering from the KTH Royal Institute of Technology, Stockholm, Sweden, in 2012, and the master's degree in mechanical engineering from Duke University, NC, USA, in 2013.

He has two years of industrial experience as a Senior Product Development Engineer with the Research and Development Department, R&D Dynamics Corporation, CT, USA, from 2013 to 2015. He has been a President's Doctoral Scholar with the Engineering Product Development Pillar, Singapore University of Technology and Design (SUTD), Singapore, since 2015. He was a Guest Research Student with the Orthopaedic Research Laboratory, Radboud University Medical Center, The Netherlands, from May 2016 to September 2016. His research interests include advanced mechanics, biomechanics, finite element method, prosthetics and orthotics design, and automotive safety design.

Mr. Shriram was a recipient of many awards including, including the Gold Medal for securing Rank 1 in bachelor's degree, in 2011, the European Commission Scholar Award, in 2011, the Duke University Scholar Award, in 2012, the Best Employee of the Year Award, in 2014, the ISMRM Educational Stipend Award, in 2016, and the ANZORS Travel Grant Award, in 2016.

GO YAMAKO received the B.S., M.S., and Ph.D. degrees from Niigata University, Japan, in 2002, 2004, and 2007, respectively. After three years of postdoctoral training at Niigata University and a medical device company, he joined the Biomechanics Research Group, University of Miyazaki, Japan, in 2010, where he is currently an Associate Professor with the Faculty of Engineering. His research interests include biomechanical engineering, orthopaedics, and sports medicine.

ETSUO CHOSA received the M.D. degree from Oita Medical University, Japan, in 1984, and the Ph.D. degree from Miyazaki Medical University, Japan. He is currently a Professor and the Chairman of the Department of Orthopaedic Surgery, Faculty of Medicine, University of Miyazaki, Japan. He does research on a wide variety of diseases, including osteoarthritis, trauma, rheumatoid arthritis, osteoporosis, and tumors. He has over 200 peer-reviewed publications in international journals and has given numerous national and international presentations.

KARUPPPASAMY SUBBURAJ received the Ph.D. degree from the IIT Bombay. He completed his postdoctoral research training at the Musculoskeletal Quantitative Imaging Research (MQIR) Laboratory, University of California at San Francisco (UCSF). He is currently an Assistant Professor and the Lead for healthcare engineering and design track with the Engineering Product Development (EPD) Pillar, Singapore University of Technology and Design (SUTD). He also leads the Medical Engineering and Design (MED) Laboratory, an interdisciplinary research group specializes in design and development of medical devices, medical imaging and image analysis methods, and computing tools for diagnosing, treating, and potentially preventing musculoskeletal disorders and disabilities. Recognizing that collaborative bridges between different disciplines are the key to advancement in today's research climate, he brings basic scientists, clinical researchers, design engineers, and physicians together to conduct clinically relevant research and translate it to patient care. His research works resulted in three patents, two books, 45 peer-reviewed technical articles in highly refereed international journals, and 75 international conference papers and presentations. He also serves as a member of the Academic Executive Committee of the Stanford-Singapore Biodesign (SSB) Program.